NATIONAL ADVISORY COMMITTEE FOR AERONAUTICS

TECHNICAL NOTE 3470

GUST-TUNNEL INVESTIGATION OF THE EFFECT OF A SHARP-EDGE GUST ON THE FLAPWISE BLADE BENDING MOMENTS OF A MODEL HELICOPTER ROTOR

By Domenic J. Maglieri and Thomas D. Reisert

Langley Aeronautical Laboratory
Langley Field, Va.

Washington

August 1955

NATIONAL ADVISORY COMMITTEE FOR AERONAUTICS

TECHNICAL NOTE 3470

GUST-TUNNEL INVESTIGATION OF THE EFFECT OF A SHARP-EDGE GUST ON THE FLAPWISE BLADE BENDING MOMENTS OF A MODEL HELICOPTER ROTOR

By Domenic J. Maglieri and Thomas D. Reisert

SUMMARY

Preliminary investigations have been made in the Langley gust tunnel to determine the effects of a sharp-edge vertical gust on the blade flapwise vibratory bending moments of small model rotors having either fixed-at-root or teetering blades. Both rotor configurations were tested up to a tip-speed ratio of about 0.35.

The results for simulated forward flight indicate that the effect of the gust on the maximum vibratory bending moment is of less importance for the teetering rotor than for the fixed-at-root rotor. Increasing the rotor speed decreases the magnitude of the vibratory bending moments resulting from a given gust. At a given rotor speed, the magnitude of the vibratory components due to the gust increases with increasing tip-speed ratio. Increasing the rotor speed at a constant forward velocity decreases the maximum vibratory bending moments for all conditions tested. The rate of increase of the vibratory bending moments with tip-speed ratio is approximately twice as great for the fixed-at-root rotor as for the teetering rotor.

INTRODUCTION

The effect of gusts on helicopter-blade bending moments is not well known. Experimental tests of a full-scale rotor in gusty air have been made at the Langley helicopter tower (ref. 1) for conditions which were limited by very low forward velocities produced by surface winds. In order to add to the understanding of the problem, simple tests of a rotor which was restrained from vertical motion were made in the Langley gust tunnel, where gust velocity, forward speed, and rotor speed could be controlled and measured accurately. For these tests, an idealized or sharp-edge gust was used for a single gust encounter.

The tests were made for two rotor conditions, cantilever and seesaw, hereinafter referred to as the fixed-at-root condition and the teetering condition. The fixed-at-root condition, which is not a realistic condition, was included as a matter of interest because maximum gust effects would be expected for this configuration. Time histories of blade bending strain were recorded for the controlled conditions of gust velocity, forward velocity, and rotor speed. The results of the investigations are presented in this report. No attempt is made to compare the experimental results with theoretical analyses.

SYMBOLS

V	airspeed of rotor along flight path, fps
Ω	rotor angular velocity, radians/sec
R	blade radius, ft
ΩR	rotor tip speed, fps
μ	tip-speed ratio, $\frac{V \cos \alpha}{\Omega R}$
U	gust velocity, fps
θ	blade-section pitch angle, deg
α	rotor angle of attack (angle between flight path and plane perpendicular to axis of no feathering), positive when axis is inclined rearward, deg
EI	blade flapwise bending stiffness, lb-in.^{2}
v_{hov}	induced velocity in hovering, fps

TEST APPARATUS

The apparatus used for the tests consisted of the gust-tunnel jet, the rotating arm, and the rotor assembly mounted in the Langley gust tunnel, as shown in figures 1 and 2. The Langley gust tunnel is simply an open-throat low-velocity wind tunnel which produces an 8- by 14-foot vertical jet of air that has an approximately rectangular velocity profile. (See ref. 2.)

The rotating arm of 15-foot radius was mounted on a searchlight base in the gust tunnel, and was used to impart a forward velocity to the rotor assembly through given gusts. The rotating arm was manually brought to the required speed in approximately 3/4 revolution and was then allowed to coast at a constant velocity during the rotor penetration into the gust. The forward velocity was recorded on an oscillograph.

The rotor assembly shown in figure 3 was attached to the end of the rotating arm and consisted of a two-blade rotor driven by a high-speed electric motor through a speed-reduction gear box. Rotor-speed control was obtained by use of a rheostat in the power-supply line. The physical characteristics of the rotor blades are shown in figure 4. The rotor blades were rectangular in plan form and had a radius of 15.69 inches and a chord of 1.20 inches. The blades were constructed of a rectangular aluminum spar enclosed in a cellulose-acetate material to form an NACA 0015 airfoil section. This type of construction was used in order to obtain a representative blade weight and bending stiffness. The first natural bending frequency of the nonrotating blade was 6.56 cycles per second and the damping ratio was 0.005. The damping ratio is defined as the ratio of the actual damping coefficient to the critical damping coefficient and was obtained experimentally. The blade bending stiffness of 33 lb-in.^{2} was slightly higher than that which would be obtained by dynamic scaling of a typical full-scale blade, but this factor is not considered to be of great importance for these tests. The rotor hub was constructed so that the blades could be fixed at the root in the flapping direction or be free to teeter. For both rotor configurations, drag hinges which allowed a fore-and-aft movement of the blade in the plane of rotation were provided at 2.17 percent of the rotor radius from the vertical axis of the hub.

INSTRUMENTATION

Resistance-wire strain gages were mounted on the spar of one blade so as to form complete bridges at 10.8 percent and 61.8 percent of the blade radius in order to measure bending strains in the flapwise direction (see fig. 4). The output of the strain gages was transmitted to a recording oscillograph through a slip-ring assembly on the rotor mount which consisted of silver slip rings with graphite brushes (fig. 3). The sensitivity of the entire strain-gage and recording system was obtained by a calibration of galvanometer deflection against known bending moments applied to the instrumented blade. The sensitivity for both gage stations was thereby obtained in terms of bending moment per inch of galvanometer deflection. The radial load was not simulated during the calibration since centrifugal loads cancel at each station when the top and bottom strain gages occupy adjacent arms of a bridge.

TEST PROCEDURE

The tests consisted of taking time-history records of blade bending strain as the rotor passed from smooth air into the fixed vertical gust. A record of the strain for the rotor hovering outside the gust was also taken for each test run. The following table gives the range of model test conditions along with the corresponding values for an equivalent full-scale rotor of 16-foot radius when both are assumed to be flying at the same lift coefficient:

	Model value	Scale factor	Equivalent full-scale value
Rotor radius, ft	1.31	12.2	16
Rotor speed, rpm	600 to 1,200	$1/\sqrt{12.2}$	172 to 344
Tip speed, fps	82.3 to 164.6	$\sqrt{12.2}$	288 to 576
Forward velocity, fps . .	0 to 32 (in 5 increments)	$\sqrt{12.2}$	0 to 112
Gust velocity, fps . . .	5; 7.5; 10	$\sqrt{12.2}$	17.5; 26.2; 35
Tip-speed ratio	0 to 0.35	1	0 to 0.35

The tests were conducted at a constant, relatively low blade pitch angle θ of 3° in order to decrease the possibility of encountering severe stall on the rotor blades as they entered the gust. No lateral or longitudinal cyclic pitch was applied to the rotor for these tests.

RESULTS AND DISCUSSION

Frequency Diagrams and Strain Records

Prior to the analysis of the records of bending strain, it was believed necessary to obtain resonance diagrams of the variation of the natural blade flapwise bending modes with rotor speed to determine whether resonance conditions were encountered over the large range of rotor speeds used for the tests. These plots (figs. 5(a) and 5(b)) were determined by using the procedure of reference 3 and the measured experimental nonrotating-blade frequency for both the fixed-at-root condition and the teetering condition.

Inspection of figure 5(a) for the fixed-at-root condition shows that the first mode of bending is near the 1-per-revolution aerodynamic loading

line and is of almost equal slope throughout the rotor-speed range. Therefore, some amplification of the 1-per-revolution variation in the bending traces could be expected. Resonance in the second bending mode is indicated at rotor speeds of 630 and 890 rpm. Some amplification of this mode may also appear in the bending-moment traces.

The resonance diagram for the teetering rotor shown in figure 5(b) is a combination of cantilever and pinned-end modes. In addition to the effects previously discussed for the fixed-at-root condition, other resonance conditions are indicated for the teetering rotor. These are shown to occur in the first antisymmetric mode at rotor speeds of 600 and 1,130 rpm.

Typical time-history records of blade bending strain are given in figure 6. This figure shows the strains measured on one blade at both strain-gage stations for the fixed-at-root rotor and the teetering rotor traversing a gust at a constant rotor angular velocity for a number of tip-speed ratios. These records represent the blade strains taken during steady flight outside the gust, during penetration of the rotor into the gust, and, for the lower advance ratios, during the new steady-flight condition when the rotor was completely immersed in the gust. Inspection of the time-history record of blade bending strain in figure 6(a) (station 10.8) for the fixed-at-root rotor shows the increased strain due to gust encounter and the 1-per-revolution variation which is predominant throughout the record. After the rotor has penetrated well into the gust, the vibratory bending moments again reach a new steady-state value since the rotor is simply operating at an increased angle of attack in the gust. The vibratory moments are somewhat larger than those experienced during the steady-flight condition outside the gust, and the mean bending-moment level has increased.

The 1-per-revolution variation shown on the record trace is due to the differences in velocity over the advancing and retreating blades, and its amplitude is possibly increased because of the proximity of the first bending mode to the 1-per-revolution aerodynamic forcing function indicated in figure 5(a). At the outboard strain-gage station (station 61.8), the 1-per-revolution variation is again present, with evidence of higher harmonic variations superimposed.

Examination of the time-history records of figure 6(a) for the teetering condition shows that little, if any, increase in the vibratory bending strains occurs when the gust is encountered, but that the mean bending-moment level has increased to the same extent as for the fixed-at-root condition. There is very little increase in the vibratory strains because of the blade flapping motion which alleviates a major portion of the load. For the teetering condition, figure 6(a) shows the presence of a 1-per-revolution variation (station 10.8) and also, in some cases, a 3-per-revolution variation (station 61.8) in the blade strains which is predicted by the resonance diagram of figure 5(b).

As the advance ratio increases (figs. 6(b) and 6(c)), the time spent by the rotor in the gust is decreased so that a new steady-flight condition is not reached in the gust. In reading the records, therefore, it was not possible to separate the vibratory bending moments obtained during the steady-flight condition in the gust (which is simply a rotor angle-of-attack change) from the vibratory components experienced during the transient condition when the rotor first entered the gust. Therefore, from records such as those shown in figure 6 for different forward velocities, gust velocities, and rotational speeds, the maximum amplitudes of the vibratory bending components for the steady-flight condition outside the gust and the transient condition at the time the rotor entered the gust were read. These values are represented by the maximum width of the strain envelopes. These blade vibratory bending moments for both the fixed-at-root condition and the teetering condition are shown in figures 7 to 10 plotted against the tip-speed ratio μ for various gust velocities and rotor rotational velocities.

The lowest curve of these plots indicates the variation of the maximum vibratory bending moment with tip-speed ratio for the steady-flight condition outside the gust. The upper curves, or gust curves, indicate the maximum vibratory bending moments experienced as a result of the gust encounter and the accompanying rotor angle-of-attack change. Differences between the lowest curve and any gust curve represent the increase in the maximum vibratory bending moments due to the gust at various tip-speed ratios. The points plotted near $\mu = 0$ on the gust curves represent the maximum vibratory bending moments that would be experienced by the rotor traversing a gust at an extremely low advance ratio or forward speed. These points were obtained experimentally by recording the bending moment for the rotor hovering outside the gust and at increments of about 12 percent of the rotor-disk penetration until the rotor was completely immersed in the gust. The gust curves were not extended to include these points, since the shape of the curves in the region is unknown.

Fixed-at-Root Condition

Inspection of figures 7 and 8 shows that the vibratory bending moments increase in an orderly manner with gust velocity and that the increase is approximately linear with tip-speed ratio above $\mu = 0.10$. Further examination of these figures indicates that the gust effect is decreased with increasing rotor speed, especially at the lower tip-speed ratios. This decrease is due to the fact that, as rotational speed is increased, the blade becomes stiffer and therefore the magnitude of the vibratory bending moments is decreased. For a given rotor speed, however, the magnitude of the vibratory components due to the gust increases with increasing tip-speed ratio.

The curves of figures 7 and 8 also show that the spread between the curve for zero gust and any gust-velocity curve is fairly large for the complete range of tip-speed ratios tested. It can be concluded, therefore, that the effect of the gust on the maximum vibratory bending moments is significant for the fixed-at-root rotor.

In addition to the effects noted in the previous paragraphs, the curves for the no-gust condition in figures 7 and 8 indicate that large vibratory bending moments occur at tip-speed ratios of about 0.02 to 0.07. These vibratory moments are especially noticeable at the higher rotor speeds at the outboard strain-gage station (see fig. 8(d)). It is known that these large flapwise vibratory bending moments can occur in rotor blades in forward flight because of unsymmetrical downwash through the rotor disk. These vibratory moments have been reported to be a maximum at 20 to 30 miles per hour for a helicopter of normal disk loading (2.0 to 2.5 lb/sq ft) and normal rotational tip-speed (see ref. 4). This speed range corresponds to the transition region from hovering to forward flight, where the unsymmetrical flow through the rotor disk is large. In figures 7 and 8, the range of tip-speed ratio corresponds to a range of velocity ratio V/v_{hov} (the ratio of the forward velocity to the hovering induced velocity) of 1.0 to 2.0. Since induced flow in hovering is small because of the low blade pitch angle used for the tests, the peaks shown correspond to a low forward velocity. The results presented in figures 4 and 5 of reference 5 indicate that, for the condition of zero shaft-axis tilt ($\alpha = 0^\circ$) at a blade pitch angle θ of 2°, the maximum dissymmetry of the inflow velocity occurs at a velocity ratio of from 1.2 to 2.2.

Teetering Condition

Figures 9 and 10 show the variation of the maximum vibratory bending moments with tip-speed ratio for the teetering rotor operating at different rotor speeds through various gusts. As with the fixed-at-root rotor, the blade vibratory bending moments increase in an orderly manner with gust velocity and increase approximately linearly with tip-speed ratio above $\mu = 0.10$ at both gage stations. Also, increasing the rotor speed decreases the gust effect as for the fixed-at-root condition (figs. 7 and 8). At a given rotor speed, the magnitude of the vibratory moments increases with increasing tip-speed ratio. Comparison of the slopes of the curves of figures 7 and 8 with those of figures 9 and 10 indicates that the rate of increase of the vibratory bending moments with tip-speed ratio is approximately twice as great for the fixed-at-root rotor as for the teetering rotor. The effect on the bending moment of the highly unsymmetrical flow which occurs during the transition region from hovering to forward flight is again evident for the teetering rotor, especially at the outboard gage station (fig. 10).

The spread between the curves which depict gust and no-gust conditions is small for the complete range of tip-speed ratios tested. In the case of the teetering rotor, therefore, it can be concluded that the effect of gusts on the maximum vibratory bending moments is fairly small.

Effect of Rotor Speed

In order to show the variation of the vibratory bending moments with rotor speed alone, a cross plot was obtained from figures 7 to 10 by plotting tip-speed ratios for which the forward velocity was 25 feet per second. These results are shown in figure 11 for both the fixed-at-root and the teetering condition. It should be pointed out that continuous curves were not faired through the test points in figure 11, since the resonance diagrams of figure 5 indicate various resonance conditions within the range of rotor speeds tested. Inspection of figure 11 indicates that, at a constant forward velocity, the maximum vibratory bending moments decrease with increasing rotor speed for both rotor configurations but decrease to a greater extent in the case of the fixed-at-root condition (fig. 11(a)). The figure also points out the lower maximum vibratory bending moments experienced by the teetering rotor as compared with the fixed-at-root rotor.

Comparison of Mean and Vibratory Blade Bending Moments

As an incidental part of the tests, the relationship between the mean and vibratory bending moments for the steady-flight condition outside the gust was determined. It was found that, as would be expected, the mean bending moments for the fixed-at-root and teetering rotors were the same. In addition, the mean bending moments were approximately constant with tip-speed ratio above $\mu = 0.1$ and varied somewhat with rotational speed. At forward speeds above cruising speed, the total vibratory bending moments experienced at the inboard station were about 60 percent of the mean values for the fixed-at-root condition and 30 percent of the mean values for the teetering condition. At the outboard station, the vibratory moments amounted to about 60 or 70 percent of the mean bending moments for both configurations.

CONCLUSIONS

Gust-tunnel tests of a fixed-at-root and a teetering model helicopter rotor 31.38 inches in diameter having a blade pitch angle of 3° were made with the rotors penetrating a vertical sharp-edge gust. The flapwise vibratory bending moments were measured at two strain-gage stations

located at 10.8 percent and 61.8 percent of the blade radius. On the basis of the results obtained, the following conclusions are drawn:

1. The vibratory bending moments increase in an orderly manner with gust velocity and the accompanying rotor angle-of-attack change for both configurations at all test conditions.

2. At a given rotor speed, the magnitude of the vibratory components due to the gust increases with increasing tip-speed ratio.

3. Increasing the rotor speed decreases the magnitude of the vibratory bending moments due to the gust.

4. The rate of increase of the vibratory bending moments with tip-speed ratio is approximately twice as great for the fixed-at-root rotor as for the teetering rotor.

5. Increasing the rotor speed at a constant forward velocity decreases the maximum vibratory bending moments for all test conditions.

6. The effect of the gusts on the maximum vibratory bending moments is of less importance for the teetering rotor than for the fixed-at-root rotor.

Langley Aeronautical Laboratory,
National Advisory Committee for Aeronautics,
Langley Field, Va., May 5, 1955.

REFERENCES

1. Jewel, Joseph W., Jr., and Carpenter, Paul J.: A Preliminary Investigation of the Effects of Gusty Air on Helicopter-Blade Bending Moments. NACA TN 3074, 1954.

2. Donely, Philip: Summary of Information Relating to Gust Loads on Airplanes. NACA Rep. 997, 1950. (Supersedes NACA TN 1976.)

3. Yntema, Robert T.: Rapid Estimation of Bending Frequencies of Rotating Beams. NACA RM L54G02, 1954.

4. Hirsch, Harold: The Contribution of Higher Mode Resonance to Helicopter Rotor-Blade Bending. Jour. Aero. Sci., vol. 20, no. 6, June 1953, pp. 407-425.

5. Coleman, Robert P., Feingold, Arnold M., and Stempin, Carl W.: Evaluation of the Induced-Velocity Field of an Idealized Helicopter Rotor. NACA WR L-126, 1945. (Formerly NACA ARR L5E10.)

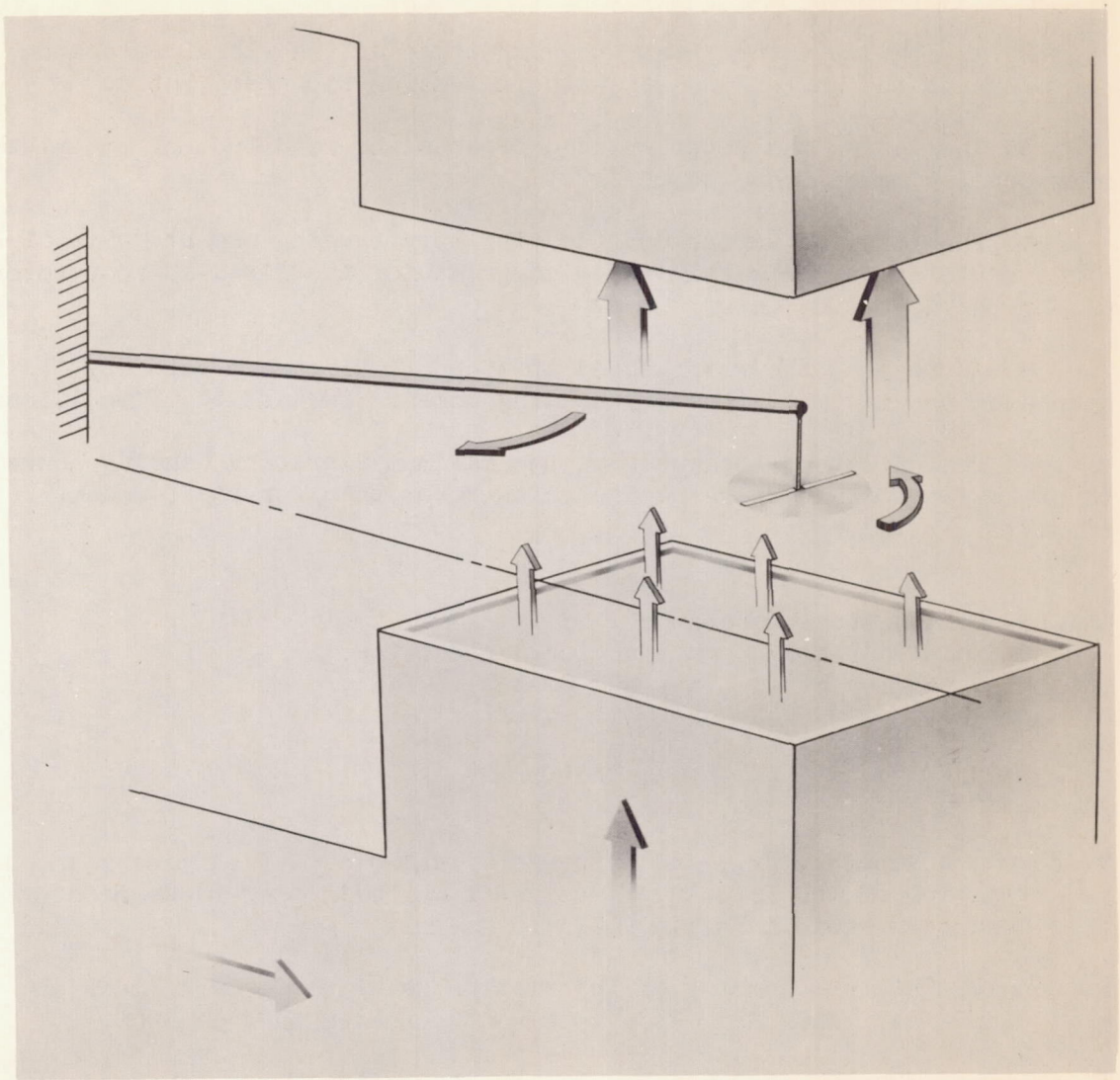

L-87968

Figure 1.- Helicopter test setup in gust tunnel.

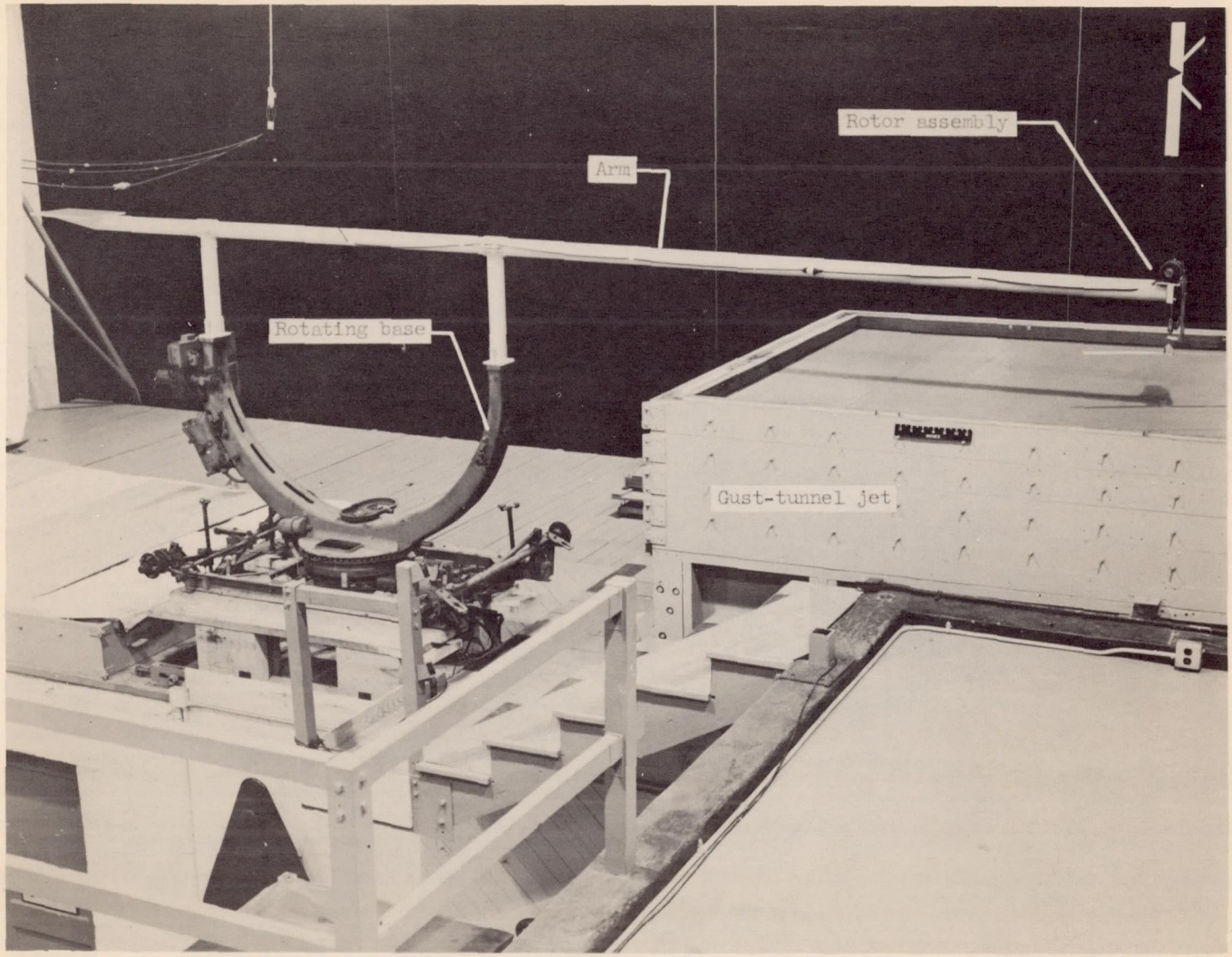

Figure 2.- Rotating base and arm assembly in the Langley gust tunnel. L-79580.1

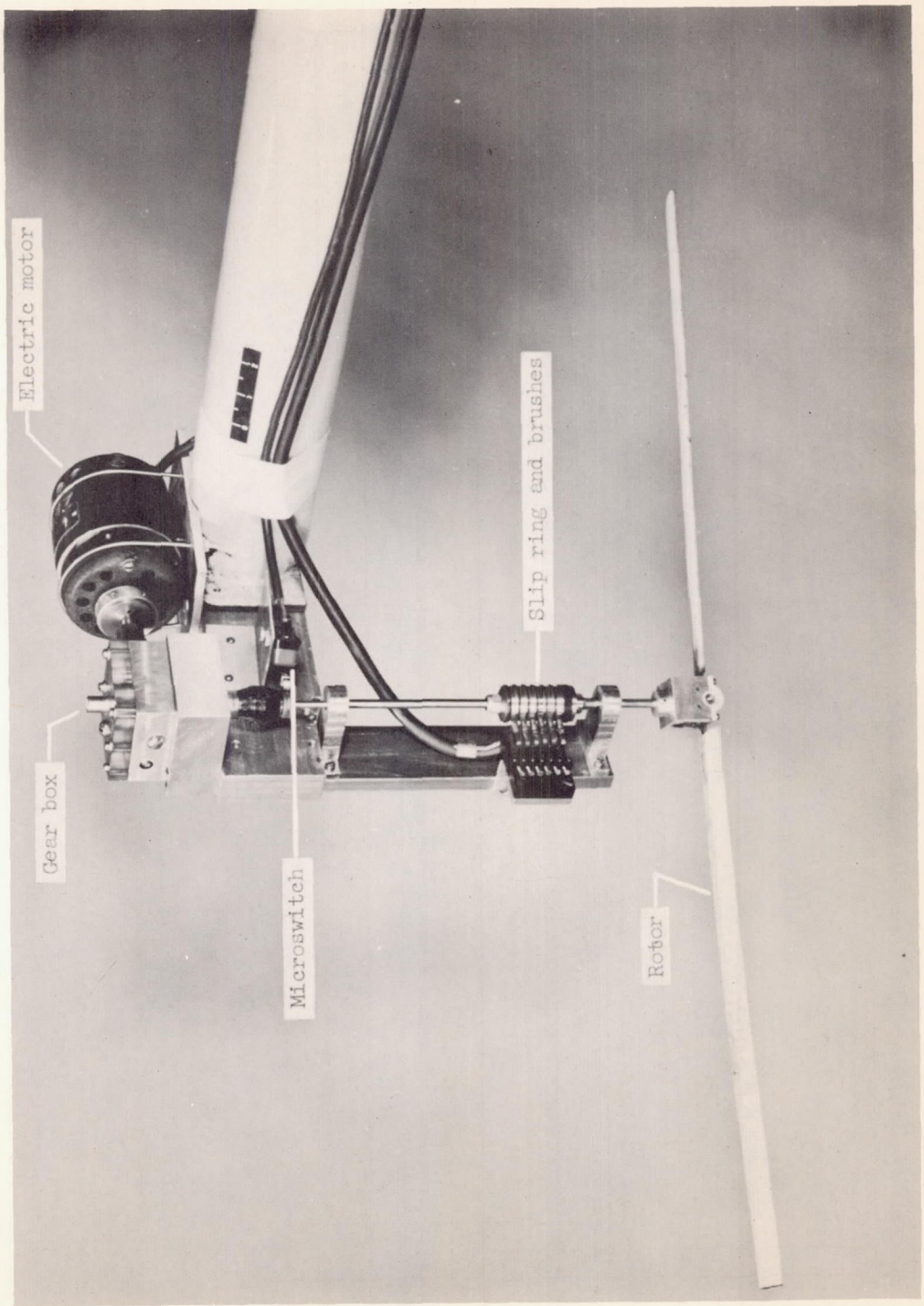

L-79579.1

Figure 3.- Slip ring and rotor assembly.

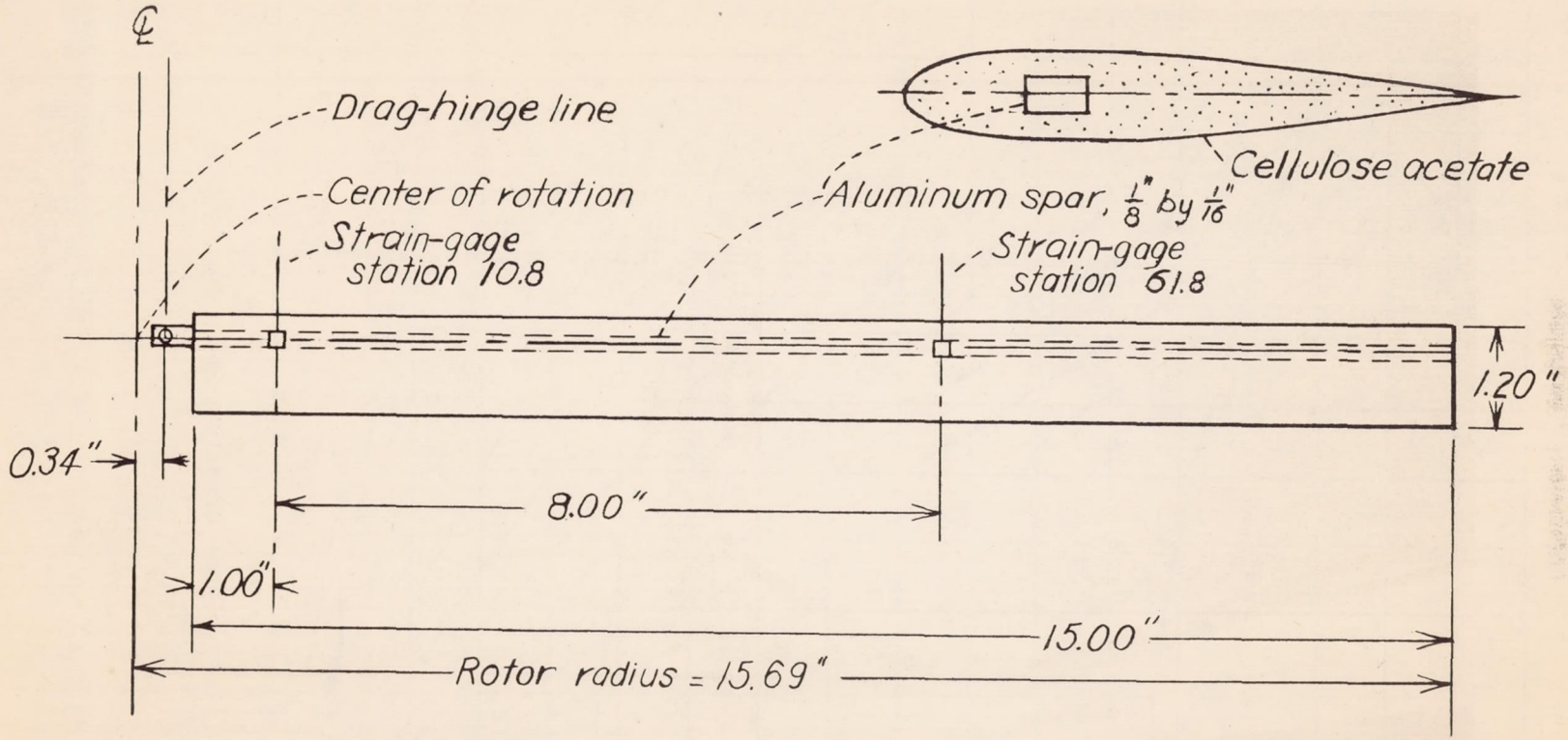

Figure 4.- Physical characteristics of rotor blades and locations of strain gages. NACA 0015 airfoil section; solidity ratio, 0.0467; blade bending stiffness, 33 lb-in.^{2}.

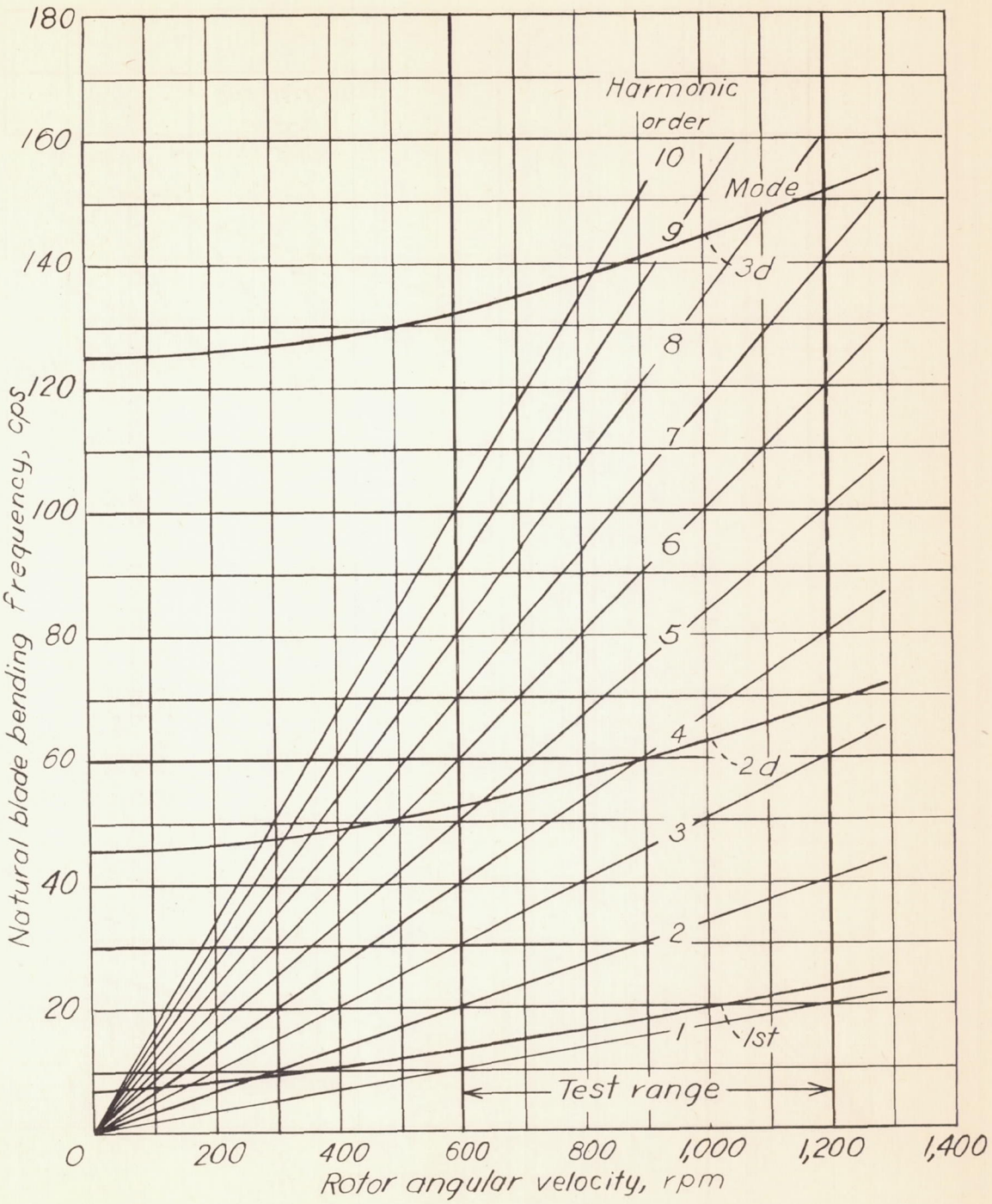

(a) Fixed-at-root condition.

Figure 5.- Variation of natural flapwise bending frequencies of rotor blade with rotational speed.

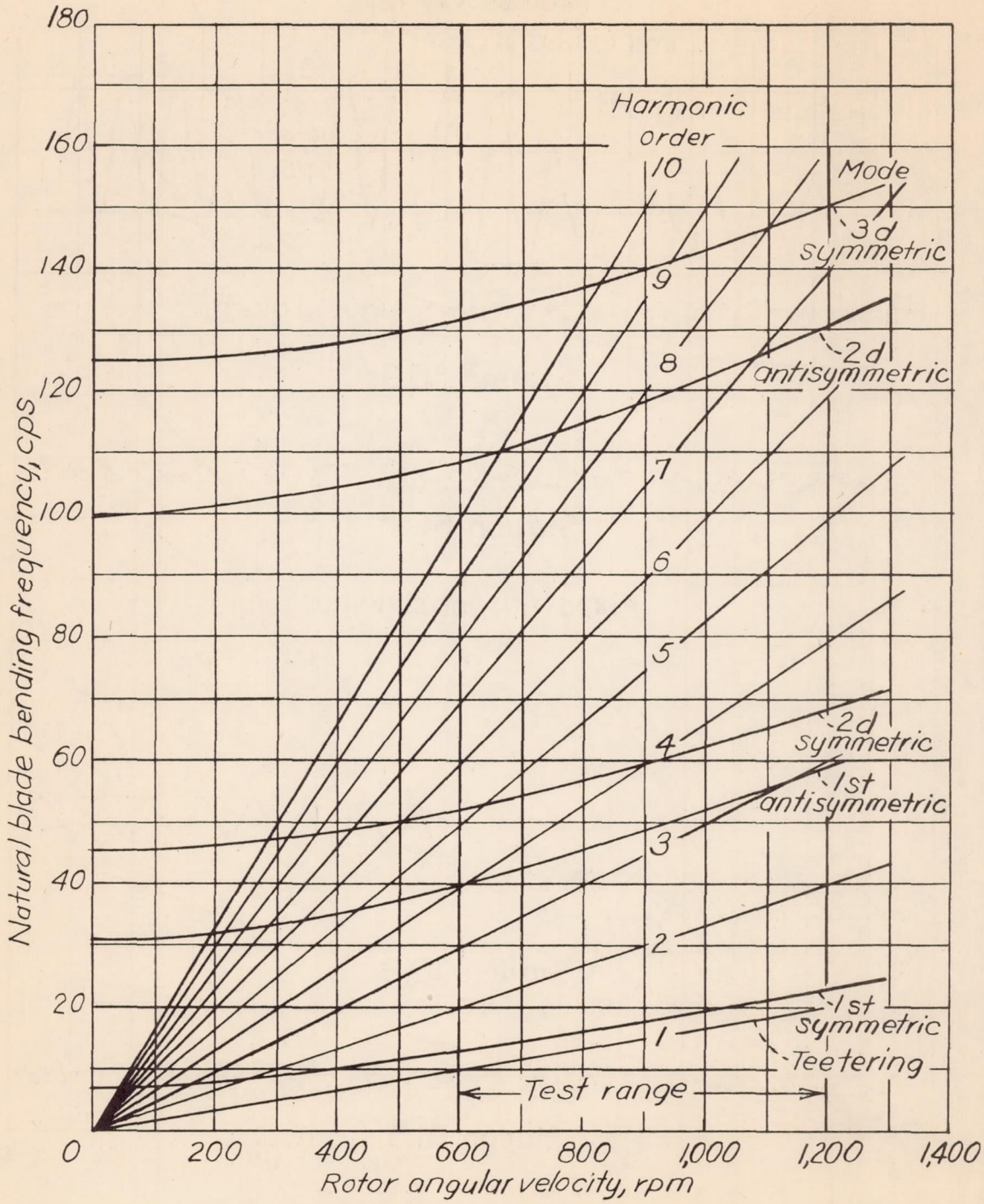

(b) Teetering condition.

Figure 5.- Concluded.

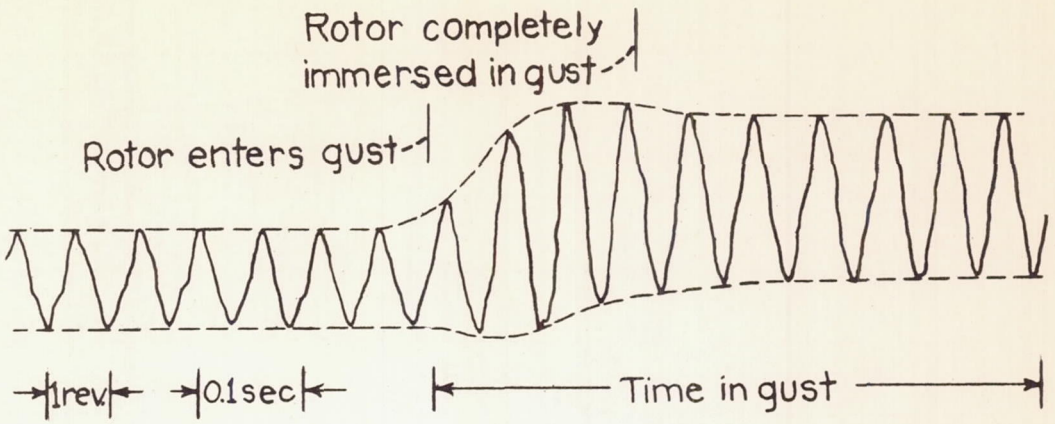

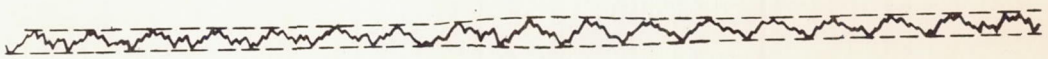

Fixed-at-root condition

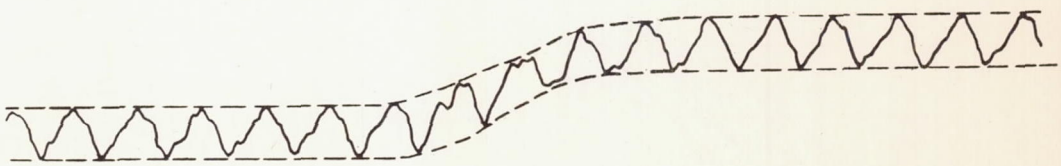

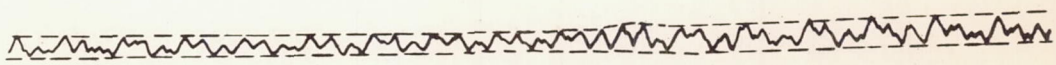

Teetering condition

(a) $\mu \approx 0.10$.

Figure 6.- Sample time-history records of blade bending strain. Ω = 1,000 rpm; θ = 3°; U = 5 fps.

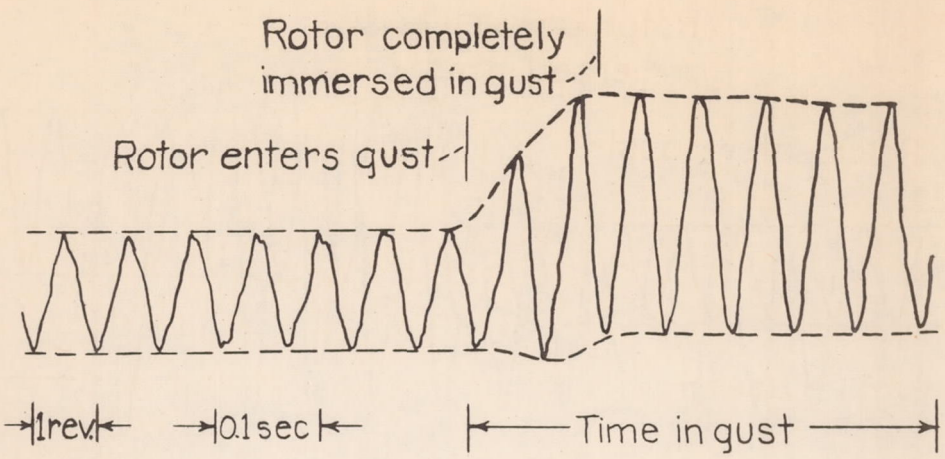

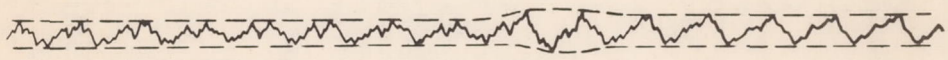

Fixed-at-root condition

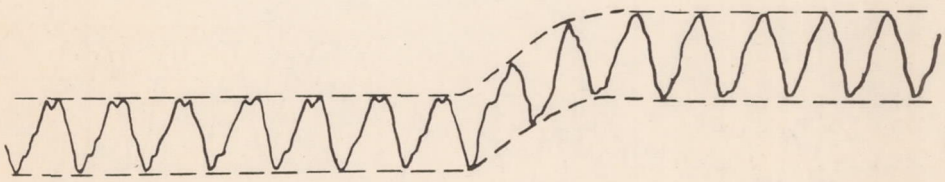

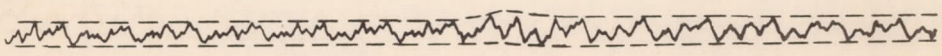

Teetering condition

(b) $\mu \approx 0.15$.

Figure 6.- Continued.

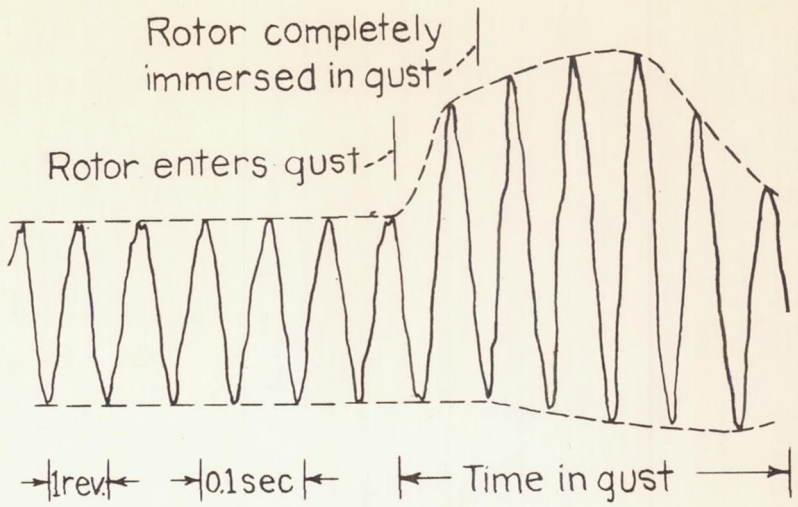

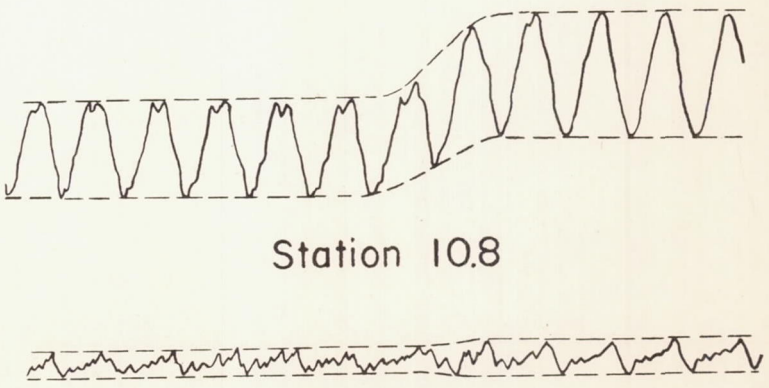

(c) $\mu \approx 0.23$.

Figure 6.- Concluded.

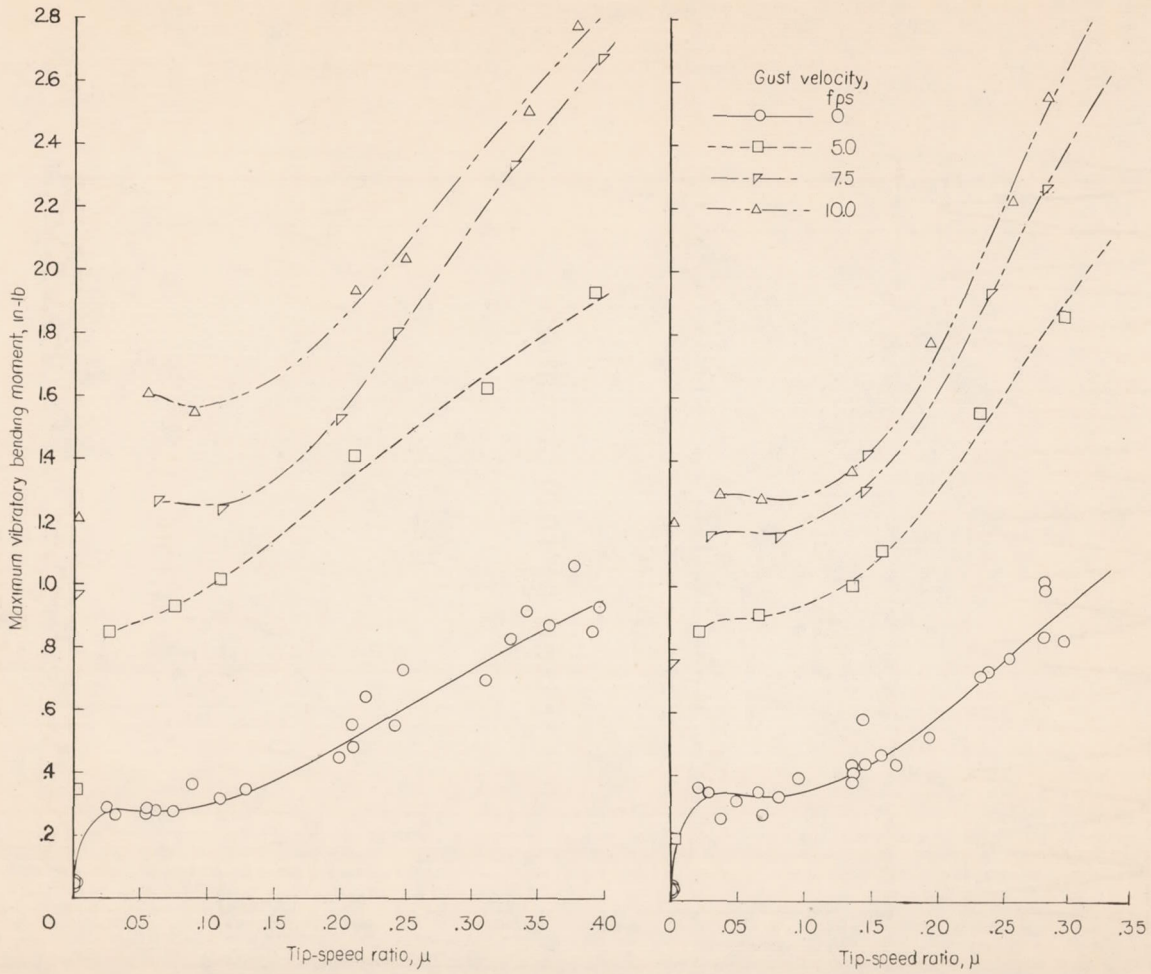

(a) 600 rpm.

(b) 800 rpm.

Figure 7.- Variation of maximum vibratory bending moment with tip-speed ratio for fixed-at-root condition (station 10.8). $\theta = 3^{\circ}$; $\alpha = 0^{\circ}$.

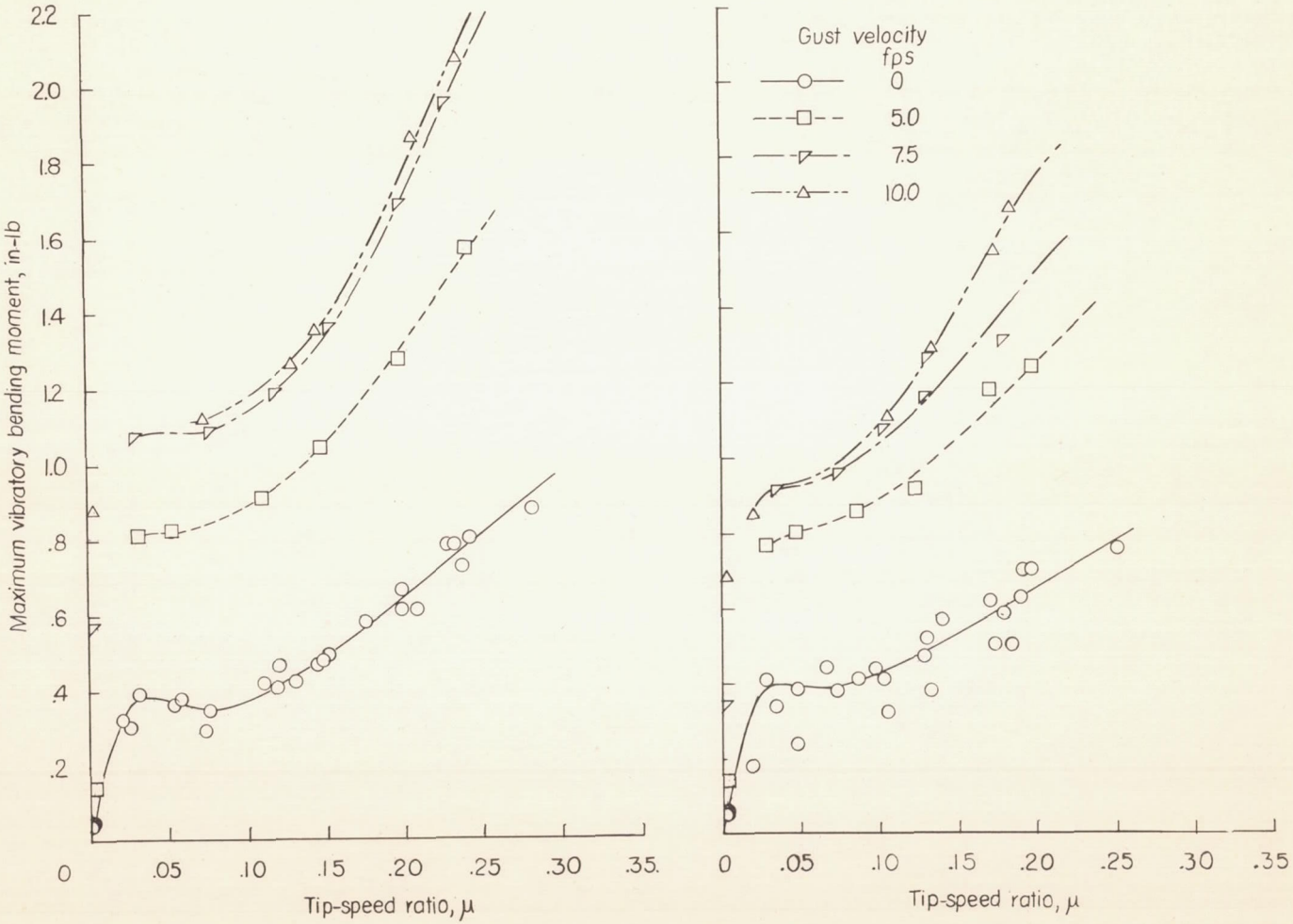

(c) 1,000 rpm.

(d) 1,200 rpm.

Figure 7.- Concluded.

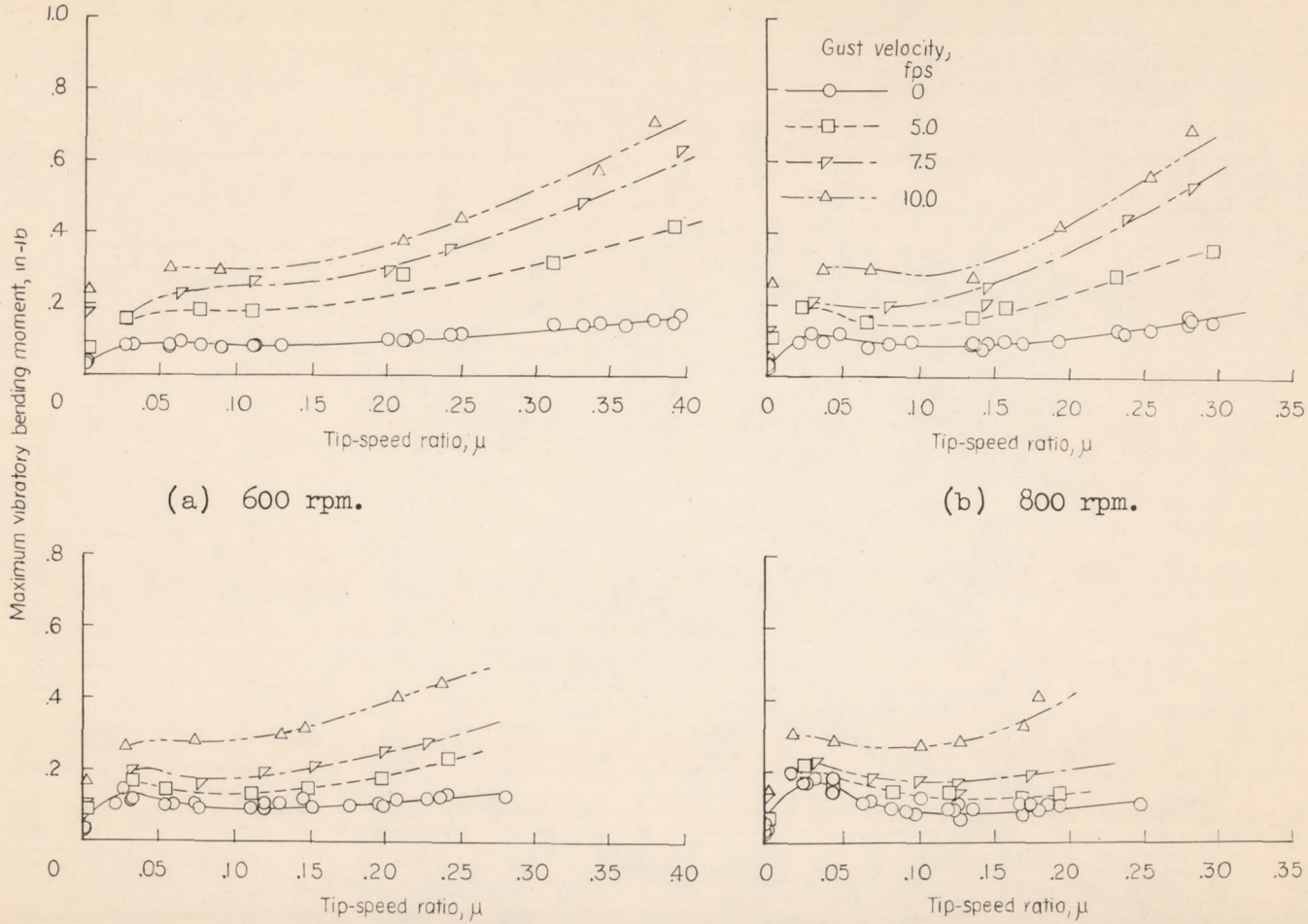

Figure 8.- Variation of maximum vibratory bending moment with tip-speed ratio for fixed-at-root condition (station 61.8). $\theta = 3^{\circ}$; $\alpha = 0^{\circ}$.

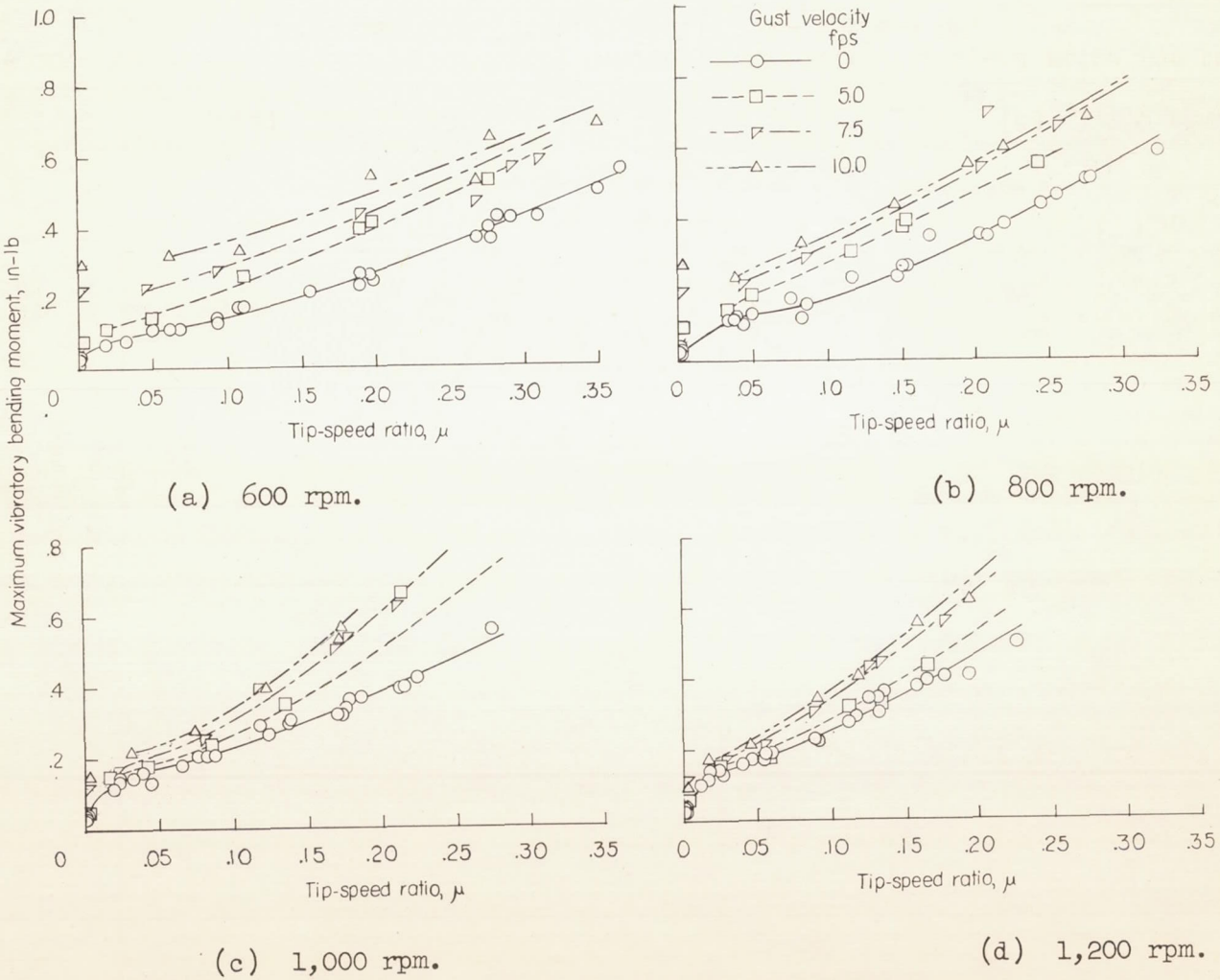

Figure 9.- Variation of maximum vibratory bending moment with tip-speed ratio for teetering condition (station 10.8). $\theta = 3^{\circ}$; $\alpha = 0^{\circ}$.

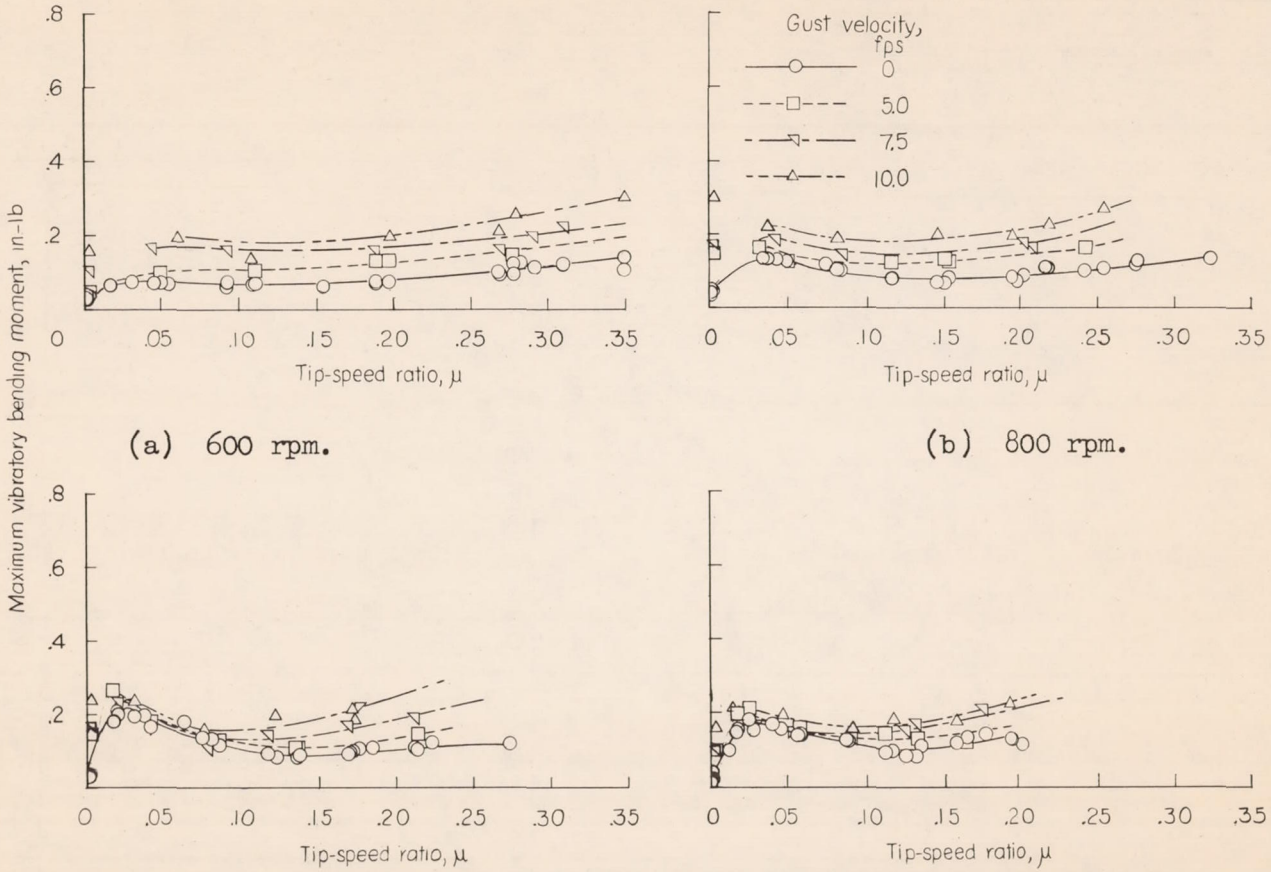

(a) 600 rpm.

(b) 800 rpm.

(c) 1,000 rpm.

(d) 1,200 rpm.

Figure 10.- Variation of maximum vibratory bending moment with tip-speed ratio for teetering condition (station 61.8). $\theta = 3^\circ$; $\alpha = 0^\circ$.

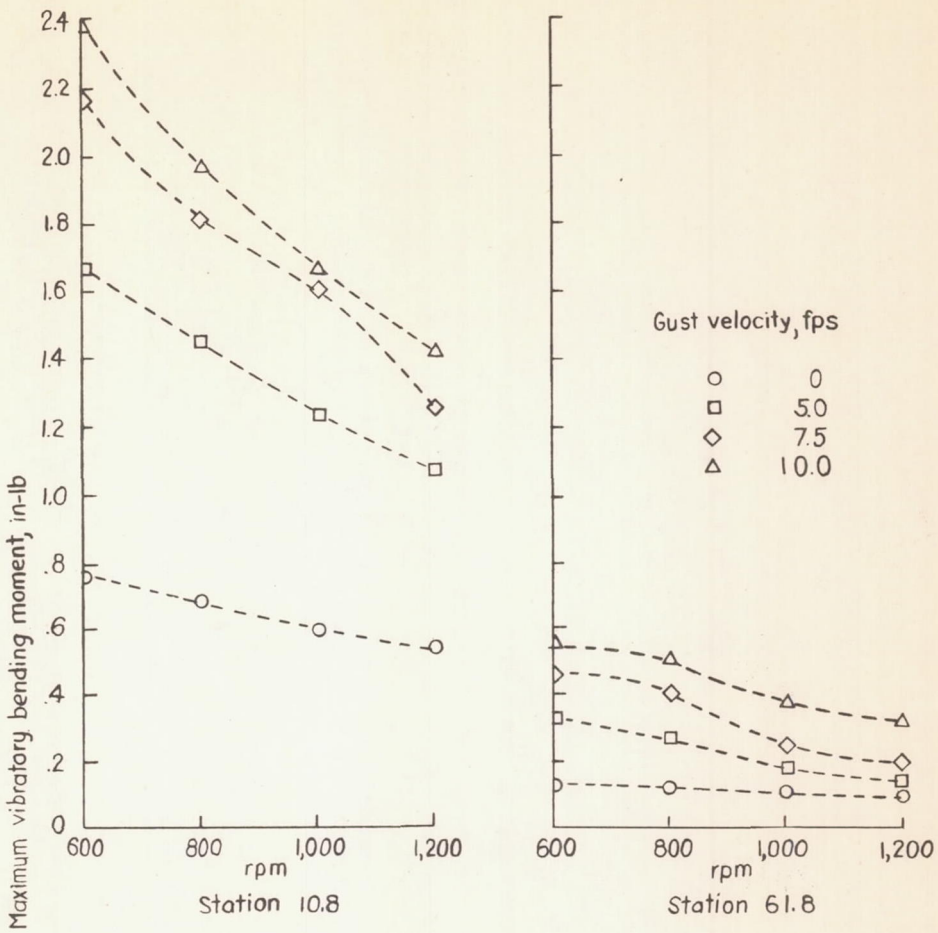

(a) Fixed-at-root condition.

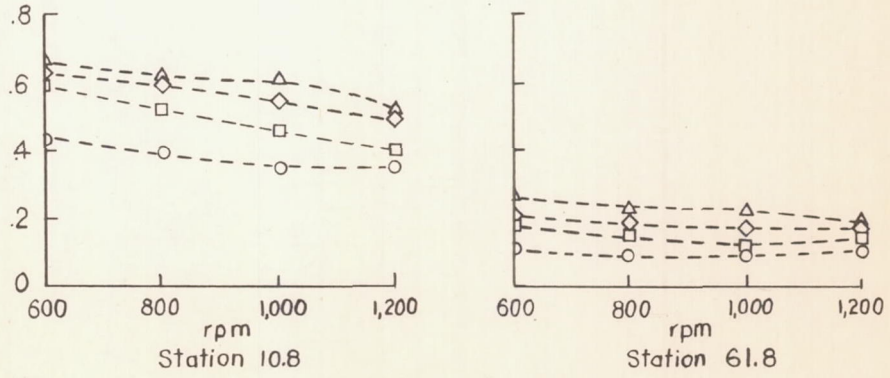

(b) Teetering condition.

Figure 11.- Variation of maximum vibratory bending moment with rotor speed. $V = 25$ fps; $\theta = 3^{\circ}$; $\alpha = 0^{\circ}$.